NPARSEC: NTT Parallaxes of Southern Extremely Cool objects. Goals, targets, procedures and first results.

R. L. Smart[1][*], C. G. Tinney[2], B. Bucciarelli[1], F. Marocco[3], U. Abbas[1], A. Andrei[4,1],
G. Bernardi[1], B. Burningham[3,4], C. Cardoso[1], E. Costa[5], M. T. Crosta[1], M. Daprá[1],
A. Day-Jones[1,5], B. Goldman[6], H. R. A. Jones[3], M. G. Lattanzi[1], S. K. Leggett[7],
P. Lucas[3], R. Mendez[5], J. L. Penna[4], D. Pinfield[3], L. Smith[3], A. Sozzetti[1],
A. Vecchiato[1]

[1]*Istituto Nazionale di Astrofisica, Osservatorio Astrofisico di Torino, Strada Osservatorio 20, 10025 Pino Torinese, Italy*
[2]*School of Physics, University of New South Wales, 2052. Australia*
[3]*Center for Astrophysics Research, University of Hertfordshire, Hatfield AL10 9AB,UK*
[4]*Observatório Nacional/MCT,R, Gal. José Cristino 77,CEP20921-400,RJ, Brazil*
[5]*Universidad de Chile,Camino el Observatorio # 1515, Santiago, Chile, Casilla 36-D*
[6]*Max Planck Institute for Astronomy, Koenigstuhl 17,D–69117 Heidelberg, Germany*
[7]*Gemini Observatory, 670 N. A'ohoku Place, Hilo, HI 96720, USA*

ABSTRACT

The discovery and subsequent detailed study of T dwarfs has provided many surprises and pushed the physics and modeling of cool atmospheres in unpredicted directions. Distance is a critical parameter for studies of these objects to determine intrinsic luminosities, test binarity and measure their motion in the Galaxy. We describe a new observational program to determine distances across the full range of T dwarf sub-types using the NTT/SOFI telescope/instrument combination. We present preliminary results for ten objects, five of which represent new distances.

Key words:

1 INTRODUCTION

The prototype T dwarf was discovered in 1995 as a companion to the nearby M dwarf star Gl229 (Nakajima et al. 1995). This was rapidly followed by many discoveries in the near-infrared Two Micron All Sky Survey (hereafter 2MASS; Skrutskie et al. 2006) and the optical Sloan Digital Sky Survey (SDSS; York et al. 2000). Once discovered, significant efforts were undertaken to determine their distances (Vrba et al. 2004; Dahn et al. 2002; Tinney et al. 2003, hereafter TIN03) to map out the lower end of the Hertzsprung-Russell diagram and to constrain models. These early T-dwarf parallax programs were operating in "discovery" mode prioritising new and exciting discoveries at cooler and cooler temperatures. For this reason, in 2010, the number of faint cool T6-T8 dwarfs with measured parallaxes was more than double the number of brighter hotter T0-T5 objects per subclass (∼5 vs ∼2, see Figure 2).

The deeper United Kingdom Infrared Deep Sky Sur-

vey (UKIDSS; Lawrence et al. 2007) and the Canada-France Brown Dwarf Survey (CFBDS; Delorme et al. 2008b) programs increased the number of known T dwarfs and extended the spectral range to T9. Recently, the Wide-field Infrared Survey Explorer (WISE; Wright et al. 2010) has extended the range into Y dwarfs and found a significant number of new T dwarfs. In 2010, this larger number of confirmed T dwarfs motivated us to commence an observational program targeting parallax measurements spanning the full T dwarf range: the *NTT Parallaxes of Southern Extremely Cool* objects survey (hereafter NPARSEC).

NPARSEC's original goal was to obtain parallaxes for 65 new brown dwarfs to ultimately increase the number of objects with precisely measured parallaxes to 10 per T dwarf sub-class. This would allow us to reduce the uncertainty in spectroscopic parallaxes from the current level of 0.4 magnitudes per subclass (Marocco et al. 2010) down to the level of the estimated cosmic scatter of 0.2 magnitudes per subclass (Smart 2009). In practice, a higher than expected observing efficiency, combined with a significantly larger pool of bright
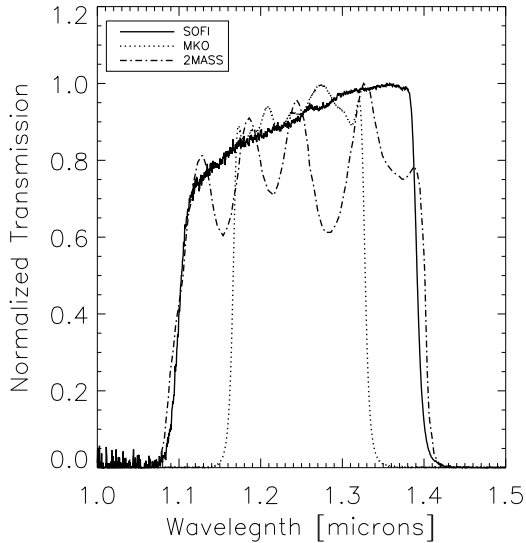
Figure 1. The SOFI J passband compared to the MKO and 2MASS bands all normalised to the maximum transmission and with no atmospheric absorption.

T dwarfs discovered in the WISE survey, have enabled us to increase our NPARSEC survey sample to 85 targets.

This sample will be used to calibrate the absolute magnitude-spectral type relation that is critical for determining distances of larger samples used in the determination of the Initial Mass Function and other statistical properties of the brown dwarf population. The distances will be used to discover and characterise peculiar objects and unresolved binaries where the spectroscopic parallax relations for normal disk brown dwarfs are not reliable. Distances are also needed to characterise **benchmark systems - e.g. systems that provide constraints on physical characteristics such as mass, age or metallicity - which,** given the degeneracy between age and spectral type for brown dwarfs, are crucial to understand the various stages of T dwarf evolution. The PARSEC program (Andrei et al. 2011), being conducted by the same team, is a complementary program for the hotter L brown dwarfs required to attain a complete picture of sub-stellar objects.

In Section 2 we describe the observational program, in Section 3 we present the target list, in Section 4 the reduction procedures used and a discussion of the precision attained, and in Section 5 we publish results from the first two years of observations and discuss individual objects. Finally in Section 6 we discuss the future of the program and the relative merits of visitor and service mode observing for ground-based astrometry, with a view to the impact of Gaia (Perryman et al. 2001) and other large sky surveys currently underway.

2   OBSERVATIONAL PROGRAM

2.1   Telescope and detector

Observations were carried out using the ESO 3.5m New Technology Telescope (NTT) and its infrared spectrograph

and imaging camera SOFI (Moorwood et al. 1998). All observations were carried out in "Large Field" mode, with a pixel scale of 0.288"/pixel and a field of view of 4.9' x 4.9'. Seeing is rarely better than 0.8, so the vast majority of images are well sampled with more than 3 pixels per full-width-at-half-maximum. All observations were made in the J band which provides the best compromise between signal-to-noise and exposure time for these objects. As can be seen from Figure 1 the SOFI J band is very similar to the 2MASS J band. This telescope and instrument combination has a proven track record for parallax determination (TIN03, Neuhäuser et al. 2002).

Our goal is to obtain at least 10% distance precision on all targets. The largest distance expected for our targets is ≈ 50 pc, corresponding to a parallax of 20 mas and resulting in a net parallax precision requirement of 2.0 mas. Many targets – especially the latest ones – are much closer with an average distance of 20 pc where we will attain a relative precision of 4%.

The parallaxes and proper motions are determined from the measured coordinates using the procedures in the Torino Observatory Parallax Program (hereafter TOPP Smart et al. 2003). The parallax is determined from the equation

$$\xi_{n,m} = \xi_{n,m_o} + (t_m - t_{m_o})\mu_n + P_{\xi_m}\pi_n \qquad (1)$$

where: $\xi_{n,m}$ is the position on frame m of star n in gnomic projection standard coordinates, $(t_m - t_{m_o})$ is the time difference with respect to the base frame, P_{ξ_m} is the parallax factor of observation m, and ξ_{n,m_o}, μ_n and π_n are the base frame position, proper motion and parallax of the star n. If we assume that the observations have a symmetric distribution of parallax factors we find that the formal error in the ξ coordinate parallax from the covariance matrix of our observation equations is given by $\sqrt{\sigma_o^2/(N < P_{\xi_m}^2 >)}$, where N is the number of observations and σ_o the sigma of unit weight of the least-squares adjustment. The parallax factor in ξ varies from -1 to 1, hence with evenly distributed observations the mean $< P_\xi^2 >$ converges to 1/3, while for the coordinate parallel to declination on average converges to 1/5. As the parallax can be found from both coordinates the formal error simplifies to $\sigma_\pi \approx 1.5\sigma_o/\sqrt{N}$ or by rearranging $N \approx 2\sigma_o^2/\sigma_\pi^2$. To obtain a parallax error of 2 mas with a per-epoch precision floor of 6-7mas (see Section 4) we require 18-24 distinct epochs per target. We have therefore chosen as a mean goal obtaining 21 epochs per target.

Since the NTT is only operated in visitor mode, we optimised our target list to be as efficient as possible for full nights. Observations are scheduled on 4 nights spread over a 7 night period, i.e. one 2 night observing block, 3 nights with no observations, then another 2 night observing block. On each 2 night observing block we attempt to observe all objects on our target list near the meridian at least once, and then on the following 2 night block we repeat this sequence. The ability to split the observations over two nights allows a larger target list, improves the chances of getting at least one night without weather problems, and permits us to tailor the target selection to observing conditions. For example, when seeing is poor we concentrate on bright targets, or if the wind blows strongly from the north we concentrate on southern targets. In addition, observations on consecutive nights are of limited use, as the targets will not have moved

significantly and the general sky conditions and the instrumental setup will probably not have changed appreciably. However, between the two 2-night blocks our targets will have significantly moved: assuming an average target with a parallax of 50 mas and a proper motion of 500 mas/yr, the apparent motion will be 13 mas, i.e. more than twice our nominal precision.

The average night length in La Silla is 10.5 hours so selecting targets evenly spaced in right ascension we observe on average 10.5/24, or 44%, of our targets on each 2-night block. As we require 21 distinct epochs per target, we budget 21/2 runs per target, hence a total of 21/2 * 24/10.5 = 24 runs. We requested one observing run every 6-8 weeks for 3 years for a total of 96 nights which was granted by ESO starting 2010-10-01. This "first order" calculation does not take into account the differing night lengths, or seasonal weather differences. We have followed this plan over the first two years, and the number of observations to date (column N_E in Table 3) shows that the summer targets tend to have (on average) less epochs than the winter targets. In our current (and last) year of operation, we will tailor time requests to "round out" those objects requiring remedial treatment.

2.2 Observation procedures

During the day we collect darks to cover all possible exposure times. We obtain dome flats using the SOFI team *specialdomeflat* observing block, and each night we take sky flats. After sky flats are completed we carry out an image analysis in the area of the first target to configure the NTT's meniscus mirrors. If the seeing is particularly good, or the images later in the night particularly elliptical, we redo this image analysis. It is usually possible to begin target observations after the first image analysis has been completed even though this is often before nautical twilight. During the twilight time we concentrate on brighter targets with shorter exposure times to minimise the effect of the brighter background sky.

The observation procedure starts with a short acquisition exposure and a move-target-to-pixel shift to (420,420) – a point slightly off-center in the SOFI focal plane which avoids trying to do astrometry at the boundaries between SOFI's four quadrant read-outs. We then begin a nine-point dither pattern similar to that adopted in TIN03. At each dither point we take an exposure with detector integration time, DIT, repeated NDIT times, and saved as a single co-added file. The telescope is then dithered and a new observation begun. This pattern is repeated N times (for N=9, 18 or 27) to obtain a total integration (based on the target's published J magnitude) of DIT×NDIT×N, as shown in Table 1. This set of discrete exposure time combinations allows us to readily obtain the required dark frames in advance of each night. The total exposure times are conservative estimates to encompass a range of sky conditions and produce a signal-to-noise of at least 50 for the target in the final co-added image. Finding charts and observing block files were developed over the first few observing runs, and have remained substantially unaltered for the whole campaign.

Table 1. Exposure times as a function of magnitude

Magnitude J	DIT (s)	NDIT	N	Total Time (min)
<14.0	3	20	9	9
14. - 15.	10	6	9	9
15. - 16.	20	6	9	18
16. - 17.	30	4	9	18
17. - 18.	30	4	18	36
>18.	30	4	27	54

2.3 Target scheduling

Splitting the target list over two nights allows us to tailor the observations to sky conditions. One driver for this split is the NTT active control of the primary and secondary mirrors. At the beginning of each night we carry out an image analysis to attain the best mirror configuration for the current conditions. This is a costly process, taking 15-20 minutes, and the mirror shape remains partially a function of the altitude (elevation) of the telescope. We therefore split the targets into northern and southern groups and carry out the image analysis at the first target of the group for that night to obtain a configuration for the average elevation.

Nightly conditions often require us to override this grouping of targets, as when, for example, the NTT must observe downwind (when wind speeds lie between 12-15 ms^{-1}). Since the wind predominantly blows from the north, our split on north-south lines is systematically impacted by this restriction. Operationally, on the first night of a 2-night block we attempt to observe the northern targets, wind permitting; if this is not possible we concentrate on southern targets so that (wind permitting) we can observe the northern group on subsequent nights.

When seeing is particularly poor, the "cost" of additional exposures to achieve a signal-to-noise of 50 for faint targets becomes prohibitive. In these conditions, we therefore concentrate on bright targets with short exposure times. This criterion dominates over other concerns, as the number of bright targets is such that we cannot pick and choose as we wish to obtain a north-south split.

3 TARGET LIST

The target list was chosen from all spectroscopically confirmed T dwarfs known in 2010 October (supplemented by a few additional late L dwarfs to fill gaps in the sky coverage). Figure 2 shows the spectral type distribution of T dwarfs with published parallaxes with relative uncertainties of less than 10% at three epochs: 2010; today; and that expected at the conclusion of NPARSEC.

Our original goal was to deliver (in combination with extant published values), a total of at least 10 objects with measured parallaxes per spectral sub-class. From Figure 2 we can see that this will be possible for all but the first and last bins. The T0-T1 bins will have additional objects from the ESO 2.2m PARSEC program (Andrei et al. 2011), the Brown Dwarf Kinematics Project (hereafter BDKP, Faherty et al. 2012), the Hawaii Infrared Parallax Program (HIPP, Dupuy & Liu 2012) and the Carnegie Astrometric Planet Search program (CAPS, Shkolnik et al. 2012). The last bin and into the Y dwarfs will be filled by the UKIDSS follow-up
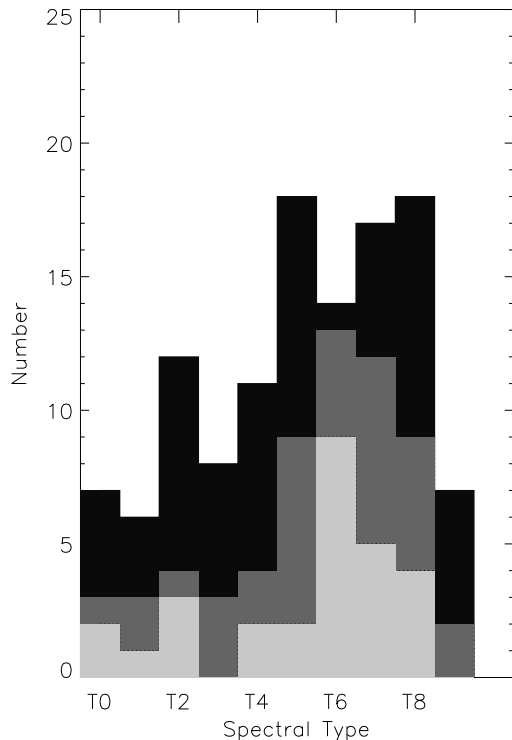
Figure 2. Number of T dwarfs with parallaxes published by 2010 in light grey, published today in dark grey and the expected NPARSEC contribution in black.

parallax program (UFPP, Smart et al. 2010) and the various Spitzer (Kirkpatrick et al. 2012; Dupuy et al. 2011) and large telescope programs (e.g. Tinney et al. 2012) currently underway.

In Table 3 we list our targets along with their published J magnitudes, infrared spectral types, estimated distances and discovery names from the original 2010 compilation. We used the published J magnitudes in the 2MASS system to derive exposure times. If the published J magnitude was in the MKO system we use Stephens & Leggett (2004) to convert it to the 2MASS system. This magnitude and the spectral type - absolute magnitude relation of Marocco et al. (2010) is used estimate the photometric distances.

4   REDUCTION PROCEDURES AND PRECISION

Flats, darks and biases are reduced using standard IRAF routines except for the dome flats where we use the SOFI team's IRAF script *special_flat.cl*. We co-add the separate dither images into one image per night using the *jitter* routine of the *Eclipse* (Devillard 1997) version 5.0 package. This routine corrects all frames using the flat fields, darks and biases. For each object's dither sequence it removes bright stars and makes the median of 7 consecutive frames to use as a sky frame to clean each dither image separately. Finally it calculates pixel offsets between each dither and applies them to produce a re-sampled and co-added final image.

The determination of positions for inclusion in the par-

allax solution from this type of sequence can be done in multiple ways. The targets in the HIPP are sufficiently bright to enable generating one position estimate per dither. In the UFPP program the centroids are measured from the final combined image. Finally, the CAPS program uses both approaches, with long integrations on the main field and a combination of short integrations on a window around the brighter targets to avoid saturation.

A naive consideration of the errors would suggest that the average of separate observations will be an improvement of $1/\sqrt{n}$ on the individual observations. However, this will only be true if each observation can be treated as an independent sample drawn from a random distribution. The processes that determine the astrometric precision of a given observation are complex and correlated within a single night. Therefore there are good reasons not to expect precision to scale simply with $1/\sqrt{n}$ within a night, nor even potentially between nights.

When considered as a inter-night problem the number of non-random factors is large: variable object fluxes, object distributions, atmospheric disturbances, optical distortions, the detector orientation / sensitivity will all contribute to correlate errors within a night. These aspects lead to a floor in the astrometric precision which multiple observations in the same night will not be able to reduce.

To test the precision of the different image treatment procedures we examined the 27 dither observations of the two targets 0148s72 and 2325s41 on the three nights 2011-08-19, 2011-11-05 and 2011-11-10. We also evaluated four centroiding routines for this data: the two dimensional Gaussian fitting procedure used in the TOPP; the Cambridge Astrometry Survey Units *imcore* maximum likelihood barycenter (CASUTOOLS, v 1.0.21); the SEXTRACTORSs barycenter; and the SEXTRACTORSs *PSFEX* psf fitting procedure (Bertin & Arnouts 1996, v. 2.8.6;).

4.1   Precision: Single Dither Observations

First we examine the centroiding precision for single dither images. We fit the positions from the 27 individual images for each night to the positions in the co-added image of the targets taken on 2011-08-19. In Figure 3 we plot the median absolute residual in the Y coordinate for 27 frames reduced using the TOPP centroiding procedures for target 0148s72 on the night of 2011-11-10. The error bars represent the root-mean-square of the residuals about the median. At bright fluxes there is a floor to the absolute residual of around 4-8 mas. At around J=14.5, the residuals slowly rise up to 12 mas at J=16.5, and thereafter deteriorate rapidly to 50 mas at J=18.5. This deterioration is due to loss of signal-to-noise for the fainter objects. Similar results are seen on the other nights and for the other target (2325s41) – though the level of the precision floor at bright fluxes did vary significantly from 4 mas to 10 mas depending on the observing conditions. The precisions obtained in these comparisons was invariant to the centroiding routine used.

4.2   Precision: Co-added Observations

We now look at how the centroiding precision improves as a function of co-adding. In Figure 4 we compare the single dither images and various co-added combinations for

Table 2. NPARSEC Targets. The J is the published J magnitude available when the program started in the 2MASS system unless indicated. The photometric distance, d_p, is calculated via the relation between absolute magnitude and spectral type provided in Marocco et al. (2010) and the J magnitude.

| Short Name	Discovery Name	Ref Dis.	Discovery α, δ hrs,deg J2000	$J \pm \sigma$	Ref J	$d_p \pm \sigma$ pc	IR SpT	Ref SpT	N_E	ΔT yr
0024n00	ULASJ002422.94+002247.9	18	0.4063721, 0.37997222	$18.16 \pm .07$	30^a	55 ± 8	T4.5	18	9	1.90
0034n05	2MASSJ00345157+0523050	8	0.5809916, 5.3847222	$15.53 \pm .05$	13	12 ± 2	T6.5	14	10	1.90
0050s33	2MASSJ00501994-3322402	11	0.8388722, -33.377833	$15.93 \pm .07$	13	12 ± 2	T7	14	11	1.90
0136n09	IPMSJ013656.57+093347.3	15	1.6157291, 9.5631444	$13.45 \pm .03$	13	6 ± 1	T2.5	15	9	1.90
0138s03	WISEPJ013836.59-032221.28	28	1.6434972, -3.3725778	$16.39 \pm .10$	13	25 ± 4	T3p	28	8	1.66
0148s72	WISEPJ014807.25-720258.75	28	1.8020139, -72.049653	$18.96 \pm .07$	28	9 ± 1	T9.5	28	9	1.68
0203s01	SDSSJ020333.26-010812.5	9	2.0592168, -1.1366389	$17.69 \pm .04$	30^a	31 ± 4	L9.5	9	10	1.90
0223s29	WISEPJ022322.34-293258.23	28	2.3895388, -29.549508	$17.34 \pm .15$	28	14 ± 2	T8	28	7	1.66
0247s16	SDSSJ024749.90-163112.6	13	2.7971611, -16.520333	$17.19 \pm .18$	13	36 ± 6	T2±1.5	13	10	1.90
0254n02	WISEPJ025409.45+022359.1	27	2.9026251, 2.3997611	$16.56 \pm .16$	27	10 ± 2	T8	28	6	0.81
0255s47	DENIS-PJ0255-4700	1	2.9176584, -47.014136	$13.25 \pm .03$	13	4 ± 1	L9	14	9	1.50
0310n16	2MASSWJ0310599+164816	3	3.1832943, 16.804306	$16.02 \pm .08$	13	16 ± 2	L9	14	12	1.89
0325n04	SDSSJ032553.17+042540.1	13	3.4314499, 4.4279444	$16.25 \pm .14$	13	20 ± 3	T5.5	13	10	1.90
0329n04	ULASJ0329+0430	29	3.4889500, 4.5068056	$17.50 \pm .03$	30^a	39 ± 6	T5	29	8	1.89
0348s60	2MASSJ03480772-6022270	7	3.8021443, -60.374169	$15.32 \pm .05$	13	9 ± 1	T7	14	9	1.17
0407n15	2MASSJ04070885+1514565	8	4.1191249, 15.249028	$16.06 \pm .09$	13	20 ± 3	T5	14	10	1.17
0415s09	2MASSIJ0415195-093506	5	4.2554278, -9.5851667	$15.69 \pm .06$	13	6 ± 1	T8	14	11	1.33
0423s04	SDSSpJ042348.57-041403.5	6	4.3968277, -4.2343056	$14.47 \pm .03$	13	9 ± 1	T0	14	9	1.58
0510s42	2MASSJ05103520-4208140	17	5.1764555, -42.137406	$16.22 \pm .09$	13	22 ± 3	T5	17	14	1.35
0516s04	2MASSJ05160945-0445499	7	5.2692919, -4.7638611	$15.98 \pm .08$	13	18 ± 3	T5.5	14	16	1.35
0518s28	2MASSJ05185995-2828372	10	5.3166528, -28.477000	$15.98 \pm .10$	13	19 ± 3	T1p	14	13	1.32
0528s33	WISEPJ052844.51-330823.98	28	5.4790306, -33.139994	$16.67 \pm .09$	28^a	10 ± 1	T8:	28	12	1.12
0542s16	WISEPJ054231.27-162829.16	28	5.7086859, -16.474767	$16.58 \pm .14$	13	16 ± 2	T7-8:	28	14	1.12
0559s14	2MASSJ05591914-1404488	2	5.9886499, -14.080222	$13.80 \pm .02$	13	7 ± 1	T4.5	14	13	1.44
0611s04	WISEPJ061135.13-041024.05	28	6.1930919, -4.1733472	$15.49 \pm .05$	13	15 ± 2	T0	28	15	1.21
0612s30	WISEPJ061213.89-303612.92	28	6.2038584, -30.603589	$17.10 \pm .19$	28	12 ± 2	T8:	28	13	1.21
0623s04	WISEPJ062309.93-045624.61	28	6.3860917, -4.9401694	$17.51 \pm .10$	28	15 ± 2	T8	28	12	1.21
0627s11	WISEPJ062720.07-111428.88	28	6.4555750, -11.241356	$15.49 \pm .05$	13	10 ± 1	T7	28	13	1.19
0727n17	2MASSIJ0727182+171001	5	7.4550667, 17.167000	$15.60 \pm .06$	13	10 ± 1	T7	16	13	1.20
0729s39	2MASSJ07290002-3954043	17	7.4833388, -39.901222	$15.92 \pm .08$	13	7 ± 1	T8pec	17	15	1.21
0751s76	WISEPJ075108.79-763449.6	28	7.8524418, -76.580444	$19.34 \pm .05$	13	17 ± 2	T9	28	7	0.33
0817s61	DENISJ081730.0-615520	23	8.2916698, -61.921056	$13.61 \pm .02$	13	5 ± 1	T6	23	9	1.13
0819s03	WISEPJ081958.05-033529.01	28	8.3327913, -3.5913917	$14.99 \pm .04$	13	13 ± 2	T4	28	17	1.32
0820n10	SDSSJ082030.12+103737.0	13	8.3417025, 10.627000	$16.98 \pm .19$	13	22 ± 4	L9.5±2	13	14	1.32
0830n01	SDSSJ083048.80+012831.1	9	8.5135498, 1.4753056	$16.29 \pm .11$	13	23 ± 4	T4.5	14	13	1.32
0926n07	ULASJ092624.76+071140.7	25	9.4402113, 7.1946389	$17.48 \pm .02$	30^a	42 ± 6	T3.5	25	10	1.32
0939s24	2MASSJ09393548-2448279	11	9.6598558, -24.807750	$15.98 \pm .11$	13	7 ± 1	T8	14	14	1.44
0949s15	2MASSJ09490860-1545485	11	9.8190556, -15.763472	$16.15 \pm .12$	13	22 ± 3	T2	14	13	1.45
0950n01	ULASJ0950+0117	29	9.8464670, 1.2928611	$18.05 \pm .04$	30^a	19 ± 3	T8	29	15	1.46
1007s45	2MASSJ10073369-4555147	17	10.126025, -45.920753	$15.65 \pm .07$	13	17 ± 2	T5	17	12	1.44
1030n02	SDSSJ103026.78+021306.4	9	10.507439, 2.2182500	$17.14 \pm .02$	30^a	24 ± 3	L9.5±1	9	18	1.43
1048n09	SDSSJ104829.21+091937.8	13	10.808128, 9.3270278	$16.59 \pm .15$	13	27 ± 4	T2.5	13	14	1.36
1110n01	SDSSpJ111010.01+011613.1	6	11.169447, 1.2702778	$16.34 \pm .12$	13	21 ± 3	T5.5	16	13	1.36
1114s26	2MASSJ11145133-2618235	11	11.247592, -26.306528	$15.86 \pm .08$	13	9 ± 1	T7.5	14	12	1.38
1122s35	2MASSJ11220826-3512363	11	11.368961, -35.210083	$15.02 \pm .04$	13	13 ± 2	T2	14	13	1.37
1157n06	SDSSJ115700.50+061105.2	9	11.950136, 6.1847778	$17.08 \pm .01$	30^a	33 ± 5	T1.5	14	13	1.24
1157n09	ULASJ115759.04+092200.7	22	11.966400, 9.3668611	$16.84 \pm .01$	30^a	31 ± 4	T2.5	22	12	1.36
1202n09	ULASJ120257.05+090158.8	25	12.049181, 9.0330000	$16.80 \pm .01$	30^a	28 ± 4	T5	25	10	1.37
1207n02	SDSSJ120747.17+024424.8	4	12.129769, 2.7402500	$15.58 \pm .07$	13	15 ± 2	T0	14	13	1.37
1209s10	2MASSJ12095613-1004008	8	12.165591, -10.066889	$15.91 \pm .08$	13	20 ± 3	T3	14	15	1.52
1215s34	2MASSJ12154432-3420591	17	12.262311, -34.349850	$16.24 \pm .13$	13	23 ± 4	T4.5	17	16	1.52
1300n12	ULASJ1300+1221	26	13.011592, 12.354083	$16.69 \pm .01$	30^a	7 ± 1	T8.5	25	12	1.31
1311n01	WISEPJ131106.24+012252.4	28	13.185066, 1.3812222	$19.16 \pm .12$	28	16 ± 2	T9:	28	10	0.47
1402n08	SDSSJ140255.66+080055.2	13	14.048789, 8.0153611	$16.84 \pm .18$	13	29 ± 5	T1.5	13	17	1.45
1404s31	2MASSJ14044941-3159329	17	14.080392, -31.992517	$15.58 \pm .06$	13	17 ± 2	T2.5	17	13	1.45
1459n08	ULASJ145935.25+085751.2	25	14.993125, 8.9642222	$17.94 \pm .03$	30^a	50 ± 7	T4.5	25	11	1.44
1504n10	SDSSJ150411.63+102718.4	13	15.069878, 10.455422	$16.50 \pm .01$	30^a	15 ± 2	T7	13	11	1.31
1511n06	SDSSJ151114.66+060742.9	13	15.187406, 6.1286389	$16.02 \pm .08$	13	19 ± 3	T0±2	13	10	1.44
1521n01	SDSSJ152103.24+013142.7	9	15.350908, 1.5285000	$16.40 \pm .10$	13	25 ± 4	T2:	14	10	1.14

Table 2 – *continued*

| Short Name	Discovery Name	Ref Dis.	Discovery α, δ hrs,deg J2000	$J \pm \sigma$	Ref J	$d_p \pm \sigma$ pc	IR SpT	Ref SpT	N_E	ΔT yr
1553n15	2MASSIJ1553022+153236	5	15.883966, 15.543583	15.82 ± 0.07	13	11±2	T7	14	11	1.29
1615n13	2MASSJ16150413+1340079	17	16.251146, 13.668869	16.35 ± 0.09	13	19±3	T6	17	11	1.38
1617n18	WISEPJ161705.75+180714.0	28	16.284929, 18.120556	17.66 ± 0.08	28^a	16±2	T8	28	9	1.18
1630n08	SDSSJ163022.92+081822.0	13	16.506374, 8.3061389	16.40 ± 0.11	13	22±3	T5.5	13	11	1.38
1741n25	WISEPJ1741+2553	28	17.690071, 25.888753	16.45 ± 0.10	28	4±1	T9	28	10	1.20
1750n17	SDSSpJ175032.96+175903.9	6	17.842480, 17.984500	16.34 ± 0.10	13	25±4	T3.5	14	13	1.37
1812n27	WISEPJ181210.85+272144.3	28	18.203014, 27.362306	18.19 ± 0.06	28^a	15±2	T8.5	28	7	1.18
1821n14	2MASSJ18212815+1414010	24	18.357819, 14.233611	13.43 ± 0.02	24	10±1	L4.5	24	7	1.20
1828s48	2MASSJ18283572-4849046	8	18.476589, -48.817944	15.18 ± 0.06	13	12±2	T5.5	14	14	1.90
1934s21	CFBDSJ193430-214221	19	19.575111, -21.705833	16.77 ± 0.15	13	30±5	T3.5	19	13	1.90
1936s55	2MASSJ19360187-5502322	20	19.600519, -55.042278	14.49 ± 0.04	13	16±2	L5	20	13	1.18
2018s74	WISEPJ201824.98-742326.1	28	20.306938, -74.390581	17.10 ± 0.30	b	23±5	T7	28	12	1.36
2043s15	SDSSJ204317.69-155103.4	13	20.721581, -15.850861	16.62 ± 0.16	13	21±3	L9	13	12	1.90
2047s07	SDSSJ204749.61-071818.3	9	20.797108, -7.3048889	16.95 ± 0.20	13	29±5	T0:	14	12	1.90
2052s16	SDSSJ205235.31-160929.8	13	20.876430, -16.158556	16.33 ± 0.12	13	23±3	T1±1	13	12	1.90
2124n01	SDSSJ212413.89+010000.3	9	21.403852, 0.99997222	16.03 ± 0.07	13	20±3	T5	14	13	1.90
2139n02	2MASSJ21392676+0220226	20	21.657436, 2.3396389	15.26 ± 0.05	13	14±2	T1.5	14	9	1.90
2151s48	2MASSJ21513839-4853542	12	21.860664, -48.898389	15.73 ± 0.08	13	19±3	T4	14	9	1.90
2154s10	2MASSJ21542494-1023022	17	21.906927, -10.383950	16.42 ± 0.12	13	25±4	T4.5	17	11	1.90
2228s43	2MASSJ22282889-4310262	7	22.474691, -43.173942	15.66 ± 0.07	13	14±2	T6	14	11	1.90
2229n01	ULASJ222958.30+010217.2	21	22.499527, 1.0381111	17.88 ± 0.04	30^a	50±7	T2.5	21	11	1.90
2239n16	WISEPJ223937.55+161716.20	28	22.660431, 16.287833	16.08 ± 0.08	13	22±3	T3	28	8	1.20
2325s41	WISEPJ232519.54-410534.90	28	23.422094, -41.093028	19.75 ± 0.05	28^a	20±3	T9	28	7	1.18
2331s47	2MASSJ23312378-4718274	8	23.523272, -47.307608	15.66 ± 0.07	13	17±2	T5	14	9	1.90
2342n08	ULASJ2342+0856	29	23.708048, 8.9389167	16.37 ± 0.01	30^a	17±2	T6.5	29	13	1.90
2356s15	2MASSIJ2356547-155310	5	23.948547, -15.886417	15.82 ± 0.06	13	17±2	T5.5	14	8	1.67

J= J band magnitude, ΔT = epoch range, d_p = photometric distance, N_E = Number of epochs todate.

Ref: 1-Martin et al. (1999), 2-Burgasser et al. (2000), 3-Kirkpatrick et al. (2000), 4-Hawley et al. (2002), 5-Burgasser et al. (2002), 6-Geballe et al. (2002), 7-Burgasser et al. (2003), 8-Burgasser et al. (2004), 9-Knapp et al. (2004), 10-Cruz et al. (2004), 11-Tinney et al. (2005), 12-Ellis et al. (2005), 13-Chiu et al. (2006), 14-Burgasser et al. (2006a), 15-Artigau et al. (2006), 16-Burgasser et al. (2006b), 17-Looper et al. (2007), 18-Lodieu et al. (2007), 19-Delorme et al. (2008a)', 20-Reid et al. (2008), 21-Chiu et al. (2008), 22-Pinfield et al. (2008), 23-Artigau et al. (2010), 24-Kirkpatrick et al. (2010), 25-Burningham et al. (2010), 26-Goldman et al. (2010), 27-Scholz et al. (2011), 28-Kirkpatrick et al. (2011), 29-Burningham et al. (2013), 30-Skrutskie et al. (2006)

Ref J Notes: a=magnitude on MKO system, b=estimated from first NPARSEC observation.
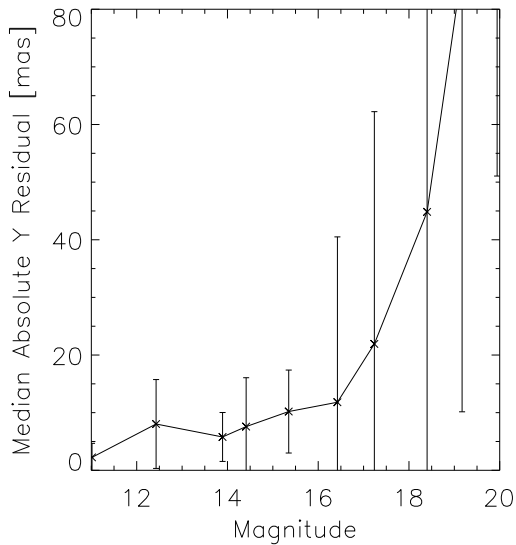
Figure 3. Absolute residuals of single dither observations for the field 0148s72 on the night of 2011-11-10 compared to the coadded image from the night of 2011-08-19. The solid line connects the median residuals in equal magnitude bins.
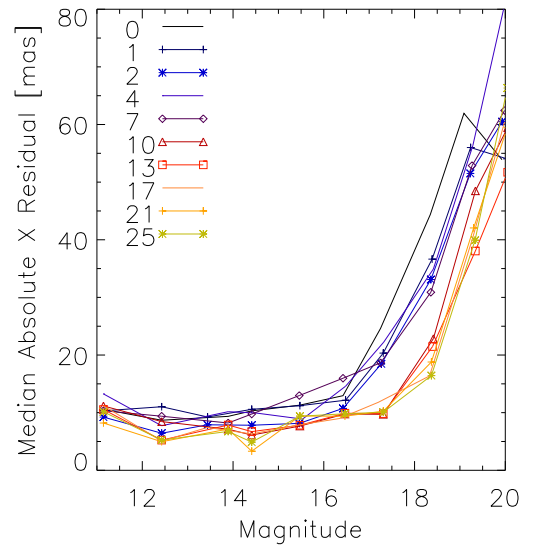
Figure 4. Absolute residuals of single dither observations (0 co-adds) and co-added combinations as shown in the legends of dithered observations for the field 0148s72 on the night of 2011-11-10 compared to the co-added image from the night of 2011-08-19.
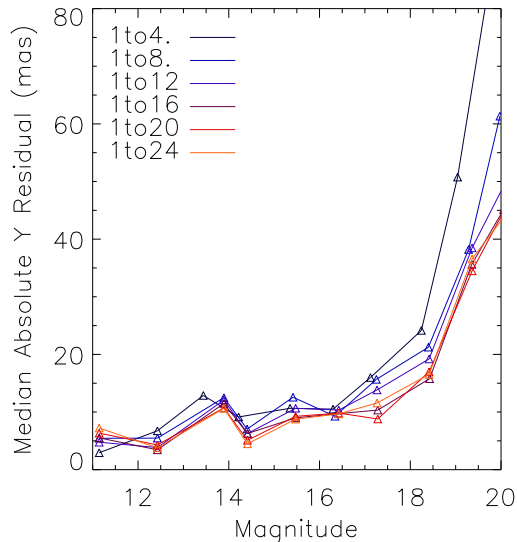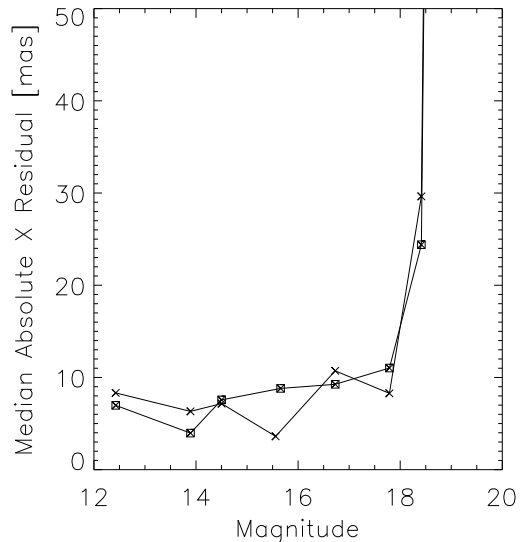
Figure 5. As Figure 4 but with first co-added image always frame 1 and the number of co-added images shown in the legend.

Figure 6. A comparison of 27 co-added images (squares) and the averages of the separate 27 images (crosses) for the field 0148s72 on the 2011-11-05 both compared to the co-added images of the same field on the night 2011-08-19.

the 0148s72 2011-11-10 observations. The main improvement obtained is to push the deterioration in precision to fainter magnitudes, e.g. extending the precision floor from J=11-15 (obtained with no co-adding), to J=11-17 (with >10 co-added images). Considering only flux for 20 co-added images we expect an increase of 3 magnitudes, however, this procedure adds resampling noise so an increase of only 2 magnitudes is reasonable.

Each co-added combination in Figure 4 is made up of subsets where the first image varied and this may be a source of noise. We therefore also followed the change in precision when the first frame was kept constant. In Figure 5 the first frame in the co-add is always frame 1 and the legend indicates the range of frames co-added. The sense of the results are similar to the previous test but it is cleaner because the first frame, and related systematic errors, are always in common. Note, we did not insist that the comparison objects are common to all tested sequences and this contributes to the noise seen.

4.3 Precision: Co-added Observations versus Normal Points

We now compare positions from co-added images to averages of the coordinates from single images. In this test we insist that the comparison objects are common to both comparisons, i.e. only the brighter objects detected in the single images. In Figure 6 for the field 0148s72 on night 2011-11-05 we compare the positions from 27 co-added images, and the average of the 27 separate positions to the observation of 2011-08-19. The two methods produce equal precision for the common objects and this indicates that the error floor is dominated by systematic, rather than random, errors.

4.4 Precision: Conclusions

These tests are only valid for the NTT-SOFI system and reduction procedures employed here. In particular, we are still experimenting with drizzling and fractional pixel allocation co-adding procedures. We conclude that the improvement from multiple images in the precision floor is very modest, not $1/\sqrt{n}$, and the main improvement is to increase the magnitude range for that floor. This range does not increase in step with signal-to-noise probably because of noise introduced by the co-adding process. Finally, for the bright objects, the use of averaged separate observations is not better than using a co-added image of those separate observations.

In the results published here we use the co-added images to maximize the magnitude range of the precision floor which we find to be around 6-7 mas. The exposures times are selected to ensure that all our targets achieve this precision.

5 PRELIMINARY RESULTS

In Table 3 we report preliminary results from the first two years of observations for 10 of our targets. The parallax determination procedures are substantially the same as those used in Smart et al. (2003). There are two differences in the application for this program: (I) We do not correct for differential colour refraction as we are working in a wavelength region where this effect is negligible (Jao et al. 2011). (II) The correction from relative to absolute parallax (COR in Table 3) is calculated using the model of Mendez & van Altena (1996) transformed into the J band which we conservatively estimate to have an error of 30% (Smart et al. 1997). Five of the objects in Table 3 overlap with published targets (see Table 4). Our results are in reasonable agreement, with some exceptions which are discussed in the following sub-sections.

Table 3. Preliminary parallaxes and proper motions for NPARSEC targets.

NPARSEC Name	RA (h:m:s)	Dec (°:′:″)	Epoch (yr)	Absolute π (mas)	COR (mas)	μ_α (mas/yr)	μ_δ (mas/yr)	N_*, N_e	ΔT (yr)
0310n16	3:11:00.0	+16:48:15.3	2011.64	36.9 ± 3.4	1.58	245.9 ± 4.0	6.2 ± 3.3	78, 12	1.89
1828s48	18:28:36.0	-48:49:03.7	2012.58	87.9 ± 2.0	0.83	234.6 ± 2.5	88.3 ± 2.6	278, 13	1.91
2043s15	20:43:17.7	-15:51:04.3	2011.62	22.8 ± 4.7	1.32	43.7 ± 4.8	-109.4 ± 3.1	173, 12	1.91
2047s07	20:47:49.5	- 7:18:21.8	2012.58	33.2 ± 5.5	1.47	35.9 ± 5.2	-241.1 ± 5.0	155, 11	1.91
2139n02	21:39:27.1	+ 2:20:23.9	2012.44	101.5 ± 2.0	1.36	485.9 ± 2.0	124.8 ± 2.7	86, 9	1.91
2151s48	21:51:38.8	-48:53:56.5	2010.76	60.0 ± 3.8	1.61	414.7 ± 3.5	-201.7 ± 4.5	52, 9	1.90
2154s10	21:54:25.1	-10:23:01.6	2010.75	37.2 ± 3.5	1.62	258.0 ± 3.1	63.3 ± 5.3	54, 11	1.91
2228s43	22:28:29.0	-43:10:30.4	2011.85	92.1 ± 2.6	1.46	51.7 ± 3.2	-301.3 ± 1.6	18, 11	1.91
2342n08	23:42:28.9	+ 8:56:20.0	2010.75	34.3 ± 5.1	1.59	264.1 ± 4.4	-52.6 ± 3.0	56, 13	1.91
2356s15	23:56:54.3	-15:53:18.5	2010.75	57.9 ± 3.5	2.21	-430.3 ± 5.8	-607.9 ± 3.0	35, 8	1.67

COR = correction to absolute parallax, N_* = number of reference stars, N_e = number of epochs, ΔT = epoch range.

Table 4. Objects with previously published parallaxes

NPARSEC Name	NPARSEC Parallax	Literature Parallax	Reference
1828s48	87.9±2.0	84.0± 8.0	BDKP
2047s07	33.2±5.5	49.9± 7.9	BDKP
2151s48	60.0±3.8	50.4± 6.7	BDKP
2228s43	92.1±2.6	94.0± 7.0	BDKP
2356s15	57.9±3.5	69.0± 3.0	BDKP
"	"	74.4± 5.8	Vrba et al. (2004)

5.1 0310n16 (2MASSWJ0310599+164816)

This object was seen as a binary in HST and VLT NACO observations (Stumpf et al. 2010) with a separation of 200 mas. In Stumpf at al. they adopted a spectroscopic distance of 25 pc and assuming a face on circular orbit this would imply a 5.2 AU separation. From the change in position angle of 15.5 degrees they found a period of 72 years and hence a minimum system mass of 30 M_{Jup}. This low mass would imply a very young system, as an older system would have to be more massive to still be close to the L/T boundary. However, the hypothesis of a young age is not supported by a comparison of the space velocities to the locus of known young objects as done in Marocco et al (2010), and in an examination of the Burgasser (2007) spectrum we do not see the triangular H band, nor a significant H and K band flux enhancement, that we expect from young objects (e.g. Lucas et al. 2001). This low mass, and hence young age, constraint will be relaxed if the orbit is larger than estimated above, which will be the case if the system is inclined or if the distance is larger than assumed by Stumpf et al. Our trigonometric distance measurement is $27.1^{+3.7}_{-2.3}$ pc, larger than the adopted 25pc but not enough to change the overall conclusion.

5.2 1828s48 (2MASSJ18283572-4849046)

This object is in the BDKP program but observed over a period before NPARSEC began. We find that our parallax and proper motions (87.9±2.0 mas, 234.6±2.5 mas/yr, 88.3±2.6 mas/yr) agrees with those found in the BDKP (83.7±7.7 mas, 231.4± 0.5 mas/yr, 52.4±10.9 mas/yr) with the exception of the declination proper motion. This could be due to the short epoch coverage for both programs

(1.91 yr for NPARSEC and 1.88 yr for BDKP). The difference could also be due to orbital motion if the object turns out to be binary. However, this is unlikely as the photometric distance is the same as the astrometric one so the object does not appear over luminous.

5.3 2047s07 (SDSSJ204749.61-071818.3)

In the BDKP this object was observed on 6 nights over 1.34 years and they found a parallax and proper motion of: 49.9±7.9 mas, 48.7±11.2 mas/yr, -193.8±11.2 mas/yr while in NPARSEC with 11 nights over 1.91 years we find 33.2±5.5 mas, 35.9±5.2 mas/yr, -241.1±5.0 mas/yr. This object has a 2MASS J magnitude of 16.95 so is at the faint end of the exposure bin for J=16-17 in Table 1 hence the signal-to-noise was often close to the minimum acceptable. As shown in Figure 7 the solution is (not unexpectedly) noisy. Notwithstanding this lower precision the fit appears well constrained and we note the photometric distance is 29±5 pc which supports the NPARSEC value.

5.4 2139n02 (2MASSJ21392676+0220226)

Faherty et al. (2009) find a proper motion of +507±22 mas/yr, 123±22 mas/yr, consistent with the values found in this program. In Radigan et al. (2012) and Khandrika et al. (2013) they find evidence of a 7 hour J band variability that we will search for when we have a larger observational dataset. In Burgasser et al. (2010) they indicate this object as a strong binary L/T candidate; however, based on our distance, it does not appear to be particularly bright and the residuals to the solution shown in Figure 7 show no signatures of orbital motion, hence these observations do not support the binarity hypothesis. In addition Radigan et al. (2012) ruled out binarity at distances beyond 1.56 AU level using HST/NICMOS imaging and Khandrika et al. (2013) do not find any significant variations in radial velocities using Gemini/NIRSPEC observations.

5.5 2342n08 (ULASJ2342+0856)

This object was provided internally from the UKIDSS T-dwarf search and spectroscopically typed as a T6.5. In
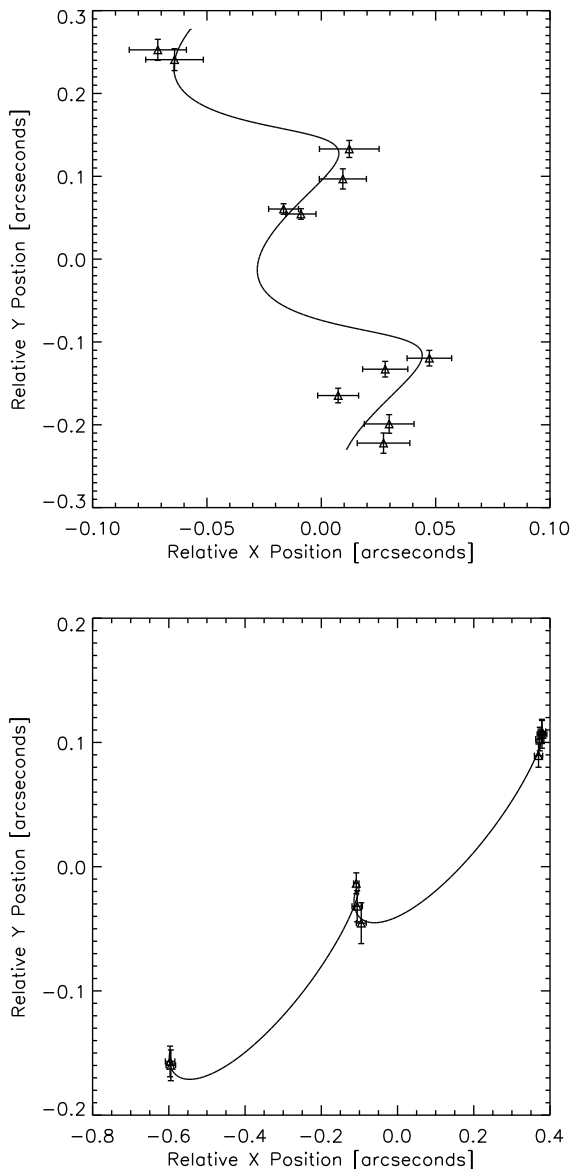
Figure 7. Example target solutions, top panel: 2047s07 with the highest error; lower panel: 2139n02 lowest error.

Scholz (2010), based on photometry, this target was indicated as a probable T7 with a proper motion of $+229\pm55$ and $-9\pm9\,$mas/yr. These proper motions are inconsistent with the NPARSEC values of 264.1 ± 4.4, $-52.6\pm3.0\,$mas/yr but in the discussion of Scholz he estimates the expected error of this object to be 48mas/yr (see his Table 5), using this value the two estimates become formally consistent.

5.6   2356s15 (2MASSIJ2356547-155310)

The NPARSEC parallax (57.9 ± 3.5 mas) is significantly smaller than the published values ($69.0\pm$ 3.0 mas and $74.4\pm$ 5.8 mas) while the NPARSEC proper motions ($-430.3\pm5.8\,$mas/yr, $-607.9\pm3.0\,$mas/yr) are in the middle of inconsistent published values ($-422.7\pm4.0\,$mas/yr, -615.9 ± 3.6 mas/yr   BDKP   and $-443\pm2\,$mas/yr,   -

$600\pm2\,$mas/yr Vrba et al. 2004). This target has the shortest NPARSEC temporal coverage (1.61 yr) and the lowest number of observations (8) in this sample so we will wait for more observations before investigating further or drawing conclusions on the difference between the published and NPARSEC values.

6   GENERAL PROGRAM CONSIDERATIONS

6.1   Visitor vs Service Programs

It is useful to compare the NPARSEC visitor program to a service program such the UFPP. Service programs provide two paths to increase the value of observations for a parallax determination: a flexibility to micro-manage scheduling, and an ability to match observations to conditions.

Scheduling flexibility in parallax observations usually translates into a request for observations at twilights when the parallax factor is an absolute maximum in ecliptic longitude, but, this is also the point where the parallax factor in the ecliptic latitude is a minimum. This is justified because the parallax factor in longitude has a larger range; the factor in latitude being usually visible at only one extreme and modulated by the sine of the latitude. However, modern programs use both coordinates to determine parallaxes so this is not a particularly strong benefit. Another plus from scheduling flexibility is, if the program is ranked high enough, to obtain a more uniform observation distribution. In NPARSEC there are seasons when we only have 2 observations of a target; in the UFPP, where our program has a high priority, we obtain over 90% of the observations requested.

Having conditions that match our requirements is undeniably an advantage. Also experienced service observers will be more efficient than the frequently changing NPARSEC observer, but, this is balanced by greater familiarity of the NPARSEC observer with the program. For the UFPP we have observations that have simple and objective constraints and all the observations to date have been useful.

A benefit in the UFPP programs is the automated reduction pipeline which has been developed as part of the UKIDSS and has used literally thousands of images to calibrate the detector. The result is a robust and precise pipeline that it is impossible to compete with using the inhomogeneous and less structured SOFI archive.

Both types of programs have different pros and cons and the final efficiency and precision will probably be dominated by the differences in the telescope/instrument combinations. The SOFI focal plane is on axis with 0.288" pixels, has been stably mounted for 15 years on the NTT which has the most advanced active optics system on a 4m-class telescope. The WFCAM focal plane is off axis with 0.4" pixels, has only been mounted for 6 years, but, it is a fixed instrument on the longest running 4m IR telescope. Since the parallaxes of brown dwarfs will remain the domain of ground based programs for the foreseeable future, this is an interesting comparison.

6.2   Large Surveys and Future Space missions

Pan-STARRS (Kaiser et al. 2002) and the future LSST surveys (LSST Science Collaboration et al. 2009), will image the sky many times a year, automatically providing the observations for parallax determination. However, surveys are managed to maximise coverage and depth; if this is done at the expense of astrometric precision or the scheduling flexibility that parallax observations require, the final precision will suffer. The 1-2 mas precision goal we have set for NPARSEC will be challenging for these large surveys, though even lower precisions with a significantly larger sample is exciting.

The impact of future astrometric space missions is promising but uncertain. The Japan Astrometry Satellite Mission for Infrared Exploration (JASMINE, Gouda et al. 2002) will measure parallaxes for thousands of T dwarfs, but the future of that mission is not clear and the precursor, Nano-JASMINE (Kobayashi et al. 2005), will not observe any T dwarfs. The Gaia mission will determine parallaxes with errors better than 0.5 mas for **all objects to Gaia magnitude 20 (de Bruijne 2012), but the only T dwarfs this bright are Epsilon Indi Ba and WISE J104915.57-531906.1AB (Luhman 2013).** Gaia will discover many T dwarfs indirectly as companions of brighter objects providing an unprecedented wealth of benchmark systems. Gaia will provide a more precise correction from the relative-to-absolute parallax for ground based parallax programs; however, as shown in Table 3, this correction is small, so the overall precision is dominated by the internal random error. Gaia will also provide an accurate reference frame which, in theory, could be used to model focal plane distortions. However, providing the focal plane does not change over the observational program, the differential nature of ground based programs uses the full precision of the observations while any modeling will introduce errors even with a perfect reference catalog, and the availability of improved Gaia accuracy may not translate into improved parallax estimates.

CONCLUSIONS AND FUTURE WORK

We have described the NPARSEC program targets, instrumentation, procedures and produced first parallaxes and proper motions for ten objects including five new objects. The observations are currently scheduled until late 2013 at which point we will publish a complete set of results. We are already finding surprises for individual targets, and we are gathering the supporting photometric and spectroscopic information to produce a complete homogenous observational data set to characterise the overall population.

ACKNOWLEDGMENTS

REFERENCES

Andrei A. H. et al., 2011, AJ, 141, 54
Artigau É., Doyon R., Lafrenière D., Nadeau D., Robert J., Albert L., 2006, ApJ, 651, L57
Artigau É., Radigan J., Folkes S., Jayawardhana R., Kurtev R., Lafrenière D., Doyon R., Borissova J., 2010, ApJ, 718, L38
Bertin E., Arnouts S., 1996, A&A, 117, 393
Burgasser A. J., 2007, ApJ, 659, 655
Burgasser A. J., Cruz K. L., Cushing M., Gelino C. R., Looper D. L., Faherty J. K., Kirkpatrick J. D., Reid I. N., 2010, ApJ, 710, 1142
Burgasser A. J., Geballe T. R., Leggett S. K., Kirkpatrick J. D., Golimowski D. A., 2006a, ApJ, 637, 1067
Burgasser A. J. et al., 2002, ApJ, 564, 421
Burgasser A. J., Kirkpatrick J. D., Cruz K. L., Reid I. N., Leggett S. K., Liebert J., Burrows A., Brown M. E., 2006b, ApJS, 166, 585
Burgasser A. J., McElwain M. W., Kirkpatrick J. D., 2003, AJ, 126, 2487
Burgasser A. J., McElwain M. W., Kirkpatrick J. D., Cruz K. L., Tinney C. G., Reid I. N., 2004, AJ, 127, 2856
Burgasser A. J. et al., 2000, AJ, 120, 1100
Burningham B. et al., 2010, MNRAS, 404, 1952
Burningham B. et al., 2013, Submitted to Mon. Not. R. Astron. Soc.
Chiu K., Fan X., Leggett S. K., Golimowski D. A., Zheng W., Geballe T. R., Schneider D. P., Brinkmann J., 2006, AJ, 131, 2722
Chiu K. et al., 2008, MNRAS, 385, L53
Cruz K. L., Burgasser A. J., Reid I. N., Liebert J., 2004, ApJ, 604, L61
Dahn C. C. et al., 2002, AJ, 124, 1170
de Bruijne J. H. J., 2012, Ap&SS, 341, 31
Delorme P. et al., 2008a, A&A, 482, 961
Delorme P. et al., 2008b, A&A, 484, 469
Devillard N., 1997, The Messenger, 87, 19
Dupuy T., Kraus A., Liu M., 2011, Spitzer Proposal, 80233
Dupuy T. J., Liu M. C., 2012, ApJS, 201, 19
Ellis S. C., Tinney C. G., Burgasser A. J., Kirkpatrick J. D., McElwain M. W., 2005, AJ, 130, 2347
Faherty J. K., Burgasser A. J., Cruz K. L., Shara M. M., Walter F. M., Gelino C. R., 2009, AJ, 137, 1
Faherty J. K. et al., 2012, ApJ, 752, 56
Geballe T. R. et al., 2002, ApJ, 564, 466
Goldman B., Marsat S., Henning T., Clemens C., Greiner J., 2010, MNRAS, 405, 1140

Gouda N. et al., 2002, in 8th Asian-Pacific Regional Meeting, Volume II, Ikeuchi S., Hearnshaw J., Hanawa T., eds., pp. 5–6

Hawley S. L. et al., 2002, AJ, 123, 3409

Jao W.-C., Henry T. J., Subasavage J. P., Winters J. G., Riedel A. R., Ianna P. A., 2011, AJ, 141, 117

Kaiser N. et al., 2002, in Society of Photo-Optical Instrumentation Engineers (SPIE) Conference Series, Vol. 4836, Society of Photo-Optical Instrumentation Engineers (SPIE) Conference Series, Tyson J. A., Wolff S., eds., pp. 154–164

Khandrika H., Burgasser A. J., Melis C., Luk C., Bowsher E., Swift B., 2013, AJ, 145, 71

Kirkpatrick J. D. et al., 2011, ApJS, 197, 19

Kirkpatrick J. D. et al., 2012, Spitzer Proposal, 90007

Kirkpatrick J. D. et al., 2010, ApJS, 190, 100

Kirkpatrick J. D. et al., 2000, AJ, 120, 447

Knapp G. R. et al., 2004, AJ, 127, 3553

Kobayashi Y. et al., 2005, in IAU Colloq. 196: Transits of Venus: New Views of the Solar System and Galaxy, Kurtz D. W., ed., pp. 491–495

Lawrence A. et al., 2007, MNRAS, 379, 1599

Lodieu N. et al., 2007, MNRAS, 379, 1423

Looper D. L., Kirkpatrick J. D., Burgasser A. J., 2007, AJ, 134, 1162

LSST Science Collaboration et al., 2009, ArXiv e-prints

Lucas P. W., Roche P. F., Allard F., Hauschildt P. H., 2001, MNRAS, 326, 695

Luhman K. L., 2013, ApJ, 767, L1

Marocco F. et al., 2010, A&A, 524, A38+

Martin E. L., Brandner W., Basri G., 1999, Science, 283, 1718

Mendez R. A., van Altena W. F., 1996, AJ, 112, 655

Moorwood A., Cuby J.-G., Lidman C., 1998, The Messenger, 91, 9

Nakajima T., Oppenheimer B. R., Kulkarni S. R., Golimowski D. A., Matthews K., Durrance S. T., 1995, Nature, 378, 463

Neuhäuser R. et al., 2002, Astronomische Nachrichten, 323, 447

Perryman M. A. C. et al., 2001, A&A, 369, 339

Pinfield D. J. et al., 2008, MNRAS, 390, 304

Radigan J., Jayawardhana R., Lafrenière D., Artigau É., Marley M., Saumon D., 2012, ApJ, 750, 105

Reid I. N., Cruz K. L., Kirkpatrick J. D., Allen P. R., Mungall F., Liebert J., Lowrance P., Sweet A., 2008, AJ, 136, 1290

Scholz R.-D., 2010, A&A, 515, A92

Scholz R.-D., Bihain G., Schnurr O., Storm J., 2011, A&A, 532, L5

Shkolnik E. L., Anglada-Escudé G., Liu M. C., Bowler B. P., Weinberger A. J., Boss A. P., Reid I. N., Tamura M., 2012, ApJ, 758, 56

Skrutskie M. F. et al., 2006, AJ, 131, 1163

Smart R. L., 2009, MSAIt, 80, 674

Smart R. L. et al., 2010, A&A, 511, A30+

Smart R. L. et al., 2003, A&A, 404, 317

Smart R. L., Lattanzi M. G., Drimmel R., 1997, in Astrophysics and Space Science Library, Vol. 212, Wide-field spectroscopy, Kontizas E., Kontizas M., Morgan D. H., Vettolani G. P., eds., pp. 195–+

Stephens D. C., Leggett S. K., 2004, PASP, 116, 9

Stumpf M. B., Brandner W., Bouy H., Henning T., Hippler S., 2010, A&A, 516, A37

Tinney C. G., Burgasser A. J., Kirkpatrick J. D., 2003, AJ, 126, 975

Tinney C. G., Burgasser A. J., Kirkpatrick J. D., McElwain M. W., 2005, AJ, 130, 2326

Tinney C. G., Faherty J. K., Kirkpatrick J. D., Wright E. L., Gelino C. R., Cushing M. C., Griffith R. L., Salter G., 2012, ApJ, 759, 60

Vrba F. J. et al., 2004, AJ, 127, 2948

Wright E. L. et al., 2010, AJ, 140, 1868

York D. G. et al., 2000, AJ, 120, 1579